Unlocking Enhanced Gas Capture via Core Scrambling of Porous-Organic Cages

Harrison D. Root[1], Matthew J. Hurlock[2, †], Nathan R. Bays[3], Brianna M. Addison[1], Jessica Rimsza[,4]*

1. Advanced Materials Laboratory, Sandia National Laboratories, Albuquerque, NM 87123 USA
2. Nanoscale Sciences Department, Sandia National Laboratories, Albuquerque, NM 87123 USA
3. Analytical Science & Corrosion Department, Sandia National Laboratories, Albuquerque, NM 87123 USA
4. Geochemistry Department, Sandia National Laboratories, Albuquerque, NM 87123 USA

*Corresponding Author: Jessica M. Rimsza, (505)284-3389, jrimsza@sandia.gov

Keywords: porous liquids, gas capture, gas separation, porous organic cages

ABSTRACT

The demand for low-cost, low-energy, and highly selective gas capture and separations is an ongoing driver of porous material development. Porous liquids have been identified as a promising gas separation material by creating permanent porosity in inorganic solvents through inclusion of nanoporous materials that sterically exclude solvent from their internal porosity. Among the nanoporous materials that can be used to form porous liquids, porous-organic cages (POCs) have been one of the most popular due to the inherent tunability of POCs. "Scrambled" POCs with varying functionalities on the POC vertices have been developed and incorporated into porous liquid compositions, increasing their gas adsorption capacity. Another unexplored avenue to tailor the properties of porous liquids is through scrambling the functionality of the core of the POC. Therefore, we have synthesized a new POC, a CC3-OH derivative with scrambled hydroxides on the core and evaluated the impact on the CO_2 uptake capacity in silicon oil-based porous liquids using the CC3-OH derivatives as the porous host. Core scrambling of the POC resulted in a twofold increase CO_2 adsorption capacity in the porous liquid, an emergent property that is a dramatic increase beyond a linear combination of the gas adsorption capacity of the neat solvent and the POC. Density functional theory modeling of the CC3 POC and its hydroxide-based derivatives identified that free rotation of the linker hydroxide allowed for forced interaction between the CO_2 molecule and the hydroxide in the pore window. Solvation of the POC may release scrambled core

hydroxides from intramolecular bonding with a neighboring imine, allowing for increased gas uptake in the porous liquid over the neat POC. These results identify a key structural relationship of POCs that enables emergent properties in porous liquids and can guide future development of liquid phase gas capture and separation materials for environmental and industrial applications.

I. Introduction

Efficient gas capture and separation through targeted material development is critical to decreasing energy demand and cost for chemical separations[1, 2]. This requires tunability of not only the gas uptake capacity, but also gas selectivity to achieve fieldable solutions. While extended structure and crystalline sorbent materials such as metal–organic frameworks (MOFs)[3, 4] and covalent organic frameworks (COFs)[5, 6] are currently under intense investigation, small molecule sorbents offer a parallel route and robust tunability allowing for scaffolds to selectively capture target gases.

Porous organic cages (POCs) are small molecule structures that display the beneficial properties of extended porous structures (high surface area, porosity, and tunability) with the added benefit of a discrete molecular structure[7, 8]. Additionally, POCs are highly soluble in common solvents, allowing for increased processability and the ability to form crystals with a controlled size and shape[9, 10]. POCs have demonstrated extensive applications in fields of molecular sensing[11, 12], catalysis[13, 14], and separations[15, 16].

The robust solubilities of POCs allow them to be readily processed into porous liquids (PLs), a liquid-phase functional material composed of a porous host and a solvent that is sterically excluded from the interior pore space, creating a material with permanent internal porosity that can be tailored for gas capture/separation systems[17]. Four types of PLs have been identified based on the composition and structure of the porous component of the PL. Here we focus on Type II PLs, which are composed of a single solvated porous molecule in an excluded solvent and were among the first PLs to be created[17].

The synthetic tunability by POCs has been exploited to impact PL guest transport/capture by “scrambling” the functionalities on the periphery of the POC, in which a mixture of functional groups are incorporated into the POC at the vertices of the cage structure. The resulting scrambled POCs have mixtures of vertex functionalities, which alters molecular packing in solid and liquid solutions, providing unique pore sizes and geometries which are inaccessible by a single pristine

POC[18, 19]. Greenaway and coworkers have demonstrated that vertex scrambling of the cages can be used to readily tune the solubility properties, packing, and guest uptake in PL systems[20, 21]. In addition to functionalization of the POC vertices, in some systems core scrambling can occur, via mixed functionalization of the linker molecules along the edges of the POC. For example, functionalization of the core benzene moieties to include –OH groups demonstrated a profound impact on the structural and spectroscopic properties of POC systems[22].

While vertex scrambling has demonstrated influence over the functional properties of POC (and PL) systems, scrambling of the core motifs on POCs and their impact on gas capture properties of resulting PLs has been underexplored. Herein, we report the synthesis of core scrambled hydroxide derivatives of CC3 POCs, a well-known POC structure with cyclohexyl moieties on their vertices[9], as well as the resultant functional properties as CO_2 sorbent PLs. While the PLs formulated from unscrambled CC3 and CC3-OH (described previously as CC19)[23,22,24] POCs did display CO_2 uptake comparable with previous reports, the scrambled CC3-OH PLs demonstrated far superior gas uptake exceeding 110 cm^3/g (a twofold increase in uptake capacity). Density functional theory (DFT) modeling of CO_2 binding with CC3 and CC3-OH POCs was used to identify the impact of core functionalization on the CO_2 adsorption properties. These results demonstrate how core functionalization impact gas capture properties of CC3 and CC3-OH POC based liquid-phase sorbent systems and creating a new pathway for discovery of novel gas separation materials.

II. Experimental Methods

Materials. Invoil 704 was purchased from Inland Vacuum Industries, Inc. Benzene tricarbaldehye, 2-hydroxybenzene tricarbaldehyde, and R,R-Cyclohexyldiamine were purchased from Ambeed. Solvents were purchased from sigma Aldrich. $CDCl_3$ was purchased from Cambridge Isotope Laboratories, Inc. All materials were used as received without further purification.

POC Synthesis. Synthesis of CC3 and CC3-OH were performed following known literature procedures[23,24], and yielded materials with identical spectroscopic characterization. For the CC3-OH-S the following procedure was used. A 1 L round bottom flask was charged with a stir bar, cyclohexyldiamine (178 mg, 1.56 mmol), and dichloromethane (150 mL) and the resulting solution cooled to 0°C. Benzene tricarbaldehyde (81 mg, 0.50 mmol) and 2-hydroxybenzene

tricarbaldehyde (89 mg, 0.50 mmol) were dissolved in dichloromethane (150 mL) and the resulting solution was added dropwise to the cooled solution of cyclohexyldiamine over 12 hours. The resulting solution was allowed to stir at room temperature for 3 days under ambient atmosphere. After the reaction was complete, the solvent was removed *via* rotary evaporator until approximately 20 mL of dichloromethane remained. Hexane (150 mL) was added to the concentrated dichloromethane solution, resulting in the precipitation of a fine yellow powder, which was isolated by filtration and washed with hexane. The solid was dried under vacuum to yield CC3-OH-S (114 mg). ^{1}H NMR (500 MHz, $CDCl_3$) δ 8.63 – 8.55 (m), 8.24 (d), 8.20 – 8.10 (m), 7.95 – 7.82 (m), 3.30 (d), 1.64 (m).

Porous Liquid Formation. Porous liquids (PLs, Figure 1) were made through modification of our previously reported methods[25-27]. To make a uniform PL sample, the POC was added to the solvent followed by vortex stirring and sonication. For example, a 10 weight % (wt%) POC PL in Invoil 704 was made by adding 0.100 g of POC to 0.900 g of Invoil 704. The solution was then vortexed for 30 s followed by sonication for 10 min.

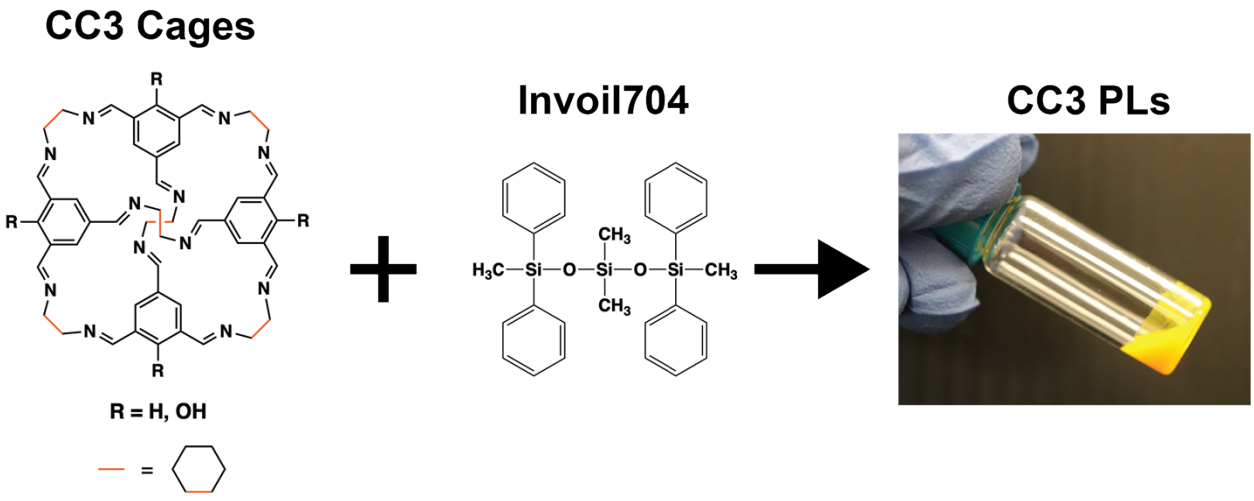

Figure 1: Schematic of CC3-based porous liquid formation.

CO_2 Gas Adsorption Analysis of Porous Liquids. Formed POC+Invoil704 PLs were analyzed at for CO_2 gas adsorption following modifications of previously reported procedures[28, 29]. Notably, stirring functionality was added for analysis of samples using a magnetic stirring plate set to a stir rate of 2. Typically, a mass of 0.2 – 0.5 g of PL samples was used for each analysis and samples

were analyzed at 0 °C and 25 °C. Temperature control of sample was done using a Micromertics chiller dewar connected to a chiller with a with a 50:50 mixture of water and ethylene glycol for the liquid bath. Single point adsorption cycling was performed six consecutive times on each sample at 25°C and a pressure of 1 bar. Between each adsorption cycle the samples were placed under dynamic vacuum (8 μbar) for 30 mins at 25 °C. PL samples were initially activated at 100°C for 8 hours and the final desorption step was performed at 25°C and 8 μbar for 1 h while stirring.

MALDI-MS. Sample preparation for matrix assisted laser desorption ionization (MALDI) mass spectrometry (MS) included the preparation of a matrix, cationizing agent, and the sample. The matrix used was 2,5-dihydroxybenzoic acid (DHBA) (>98%, Sigma-Aldrich) prepared in methanol at a concentration of 10 mg/mL. The cationizing agent used was silver trifluoroacetate (AgTFA) (1 mg/mL) and was prepared in acetonitrile at a concentration of 1 mg/mL. The sample solution was prepared in a 1:1 mixture of methanol and dichloromethane at a concentration of 1 mg/mL. All three solutions were mixed in a 1:1:1 ratio by volume and drop-cast three times per well on a MALDI plate, then allowed to fully dry for 1 hour. Additionally, several reference wells were plated by replacing the sample solution with a 1:1 mixture of methanol and dichloromethane.

Simulation Methods. All the simulations were spin-polarized projected-augmented wave (PAW) DFT calculations carried out using the Vienna Ab initio Simulations Package (VASP).[30,31] Each calculation used a 600 eV cut-off along with the PBEsol exchange-correlation functional.[32] Van der Waals interactions were included with Grimme's D3 dispersion correction.[33] Structural optimizations used an electronic convergence criterion of 10^{-5} ev and a force convergence of 0.01 eV/Å. A Gamma-point *k*-point mesh and real-space algorithm was used for all calculations. Similar computational parameters have been successfully used to evaluate gas binding in porous organic cages and metal-organic frameworks [34-40]. A CC3 POC structure was used as the base composition and was simulated inside a 25x25x25 Å simulation box to limit interactions with the periodic replicates. Structural optimization of the CC3 POC was performed, prior to the formation of the CC3-OH structures. For the CC3-OH POC hydroxides replaced a hydrogen on the benzene ring of the core on each of the four linkers. The amount of hydroxide in the system increased from 33% (on hydroxide per linker), to 66% (two hydroxides per linker), to 100% (three hydroxides per linker). Previous studies have noted that formation of intramolecular hydrogen bonds has a

significant impact on not only the structure, but also the optical and gas adsorption properties of rare-earth metal-organic frameworks[41]. Since a similar chemical structure occurs here two series of CC3 POCs were evaluated, one with the hydroxide hydrogen-bound to the neighboring imine, and the other with the hydroxides oriented away from the imine. Following optimization of the series of CC3-nOH POCs a single CO_2 molecule was placed into the POC pore and then the entire system was optimized. The procedure was repeated until the total number of CO_2 molecules in the POC was seven. Reaction free energies (ΔG) were calculated through the energy differences between the optimized CC3-OH POC + nCO_2 systems ($E_{POC\text{-}CO2}$), the combined energy of the CC3-OH POC (E_{POC}), and the energy of the isolated CO_2 molecule (E_{CO2}) as seen in Equation 1.

$$\Delta G = E_{POC-CO2} - \sum_{n=0}^{6} E_{POC} + n * E_{CO2} \quad (1)$$

To evaluate the impact of structural changes in the POC following CO_2 adsorption, single point calculations with the same parameters were calculated following relaxation of the POC + CO_2 system. This single point energy of the POC was used as E_{POC} in Eq. 1.

III. *Results*

The impact of the addition of -OH functionalization on the core of the CC3 POCs (Figure 2) was evaluated for CO_2 uptake in both the solid state and in PL systems, which evaluates their use in chemical separations[1]. CC3 and CC3-OH POCs were synthesized according to literature procedure. A slightly modified procedure, described above, was used for synthesis of the CC3-OH-S structure with cage scrambling (CC3-OH-S). Synthesis of known POCs (CC3, CC3-OH) was confirmed *via* ^{1}H NMR spectroscopy, which showed spectra consistent with previously reports[23,24]. CC3-OH-S ^{1}H NMR spectroscopy (Figure 3, S3) showed broadening and splitting of the observed proton resonances, as expected and seen in previously scrambled cages, however the presence of five cages in the system resulted in a spectrum that was difficult to deconvolute to identify each cage.

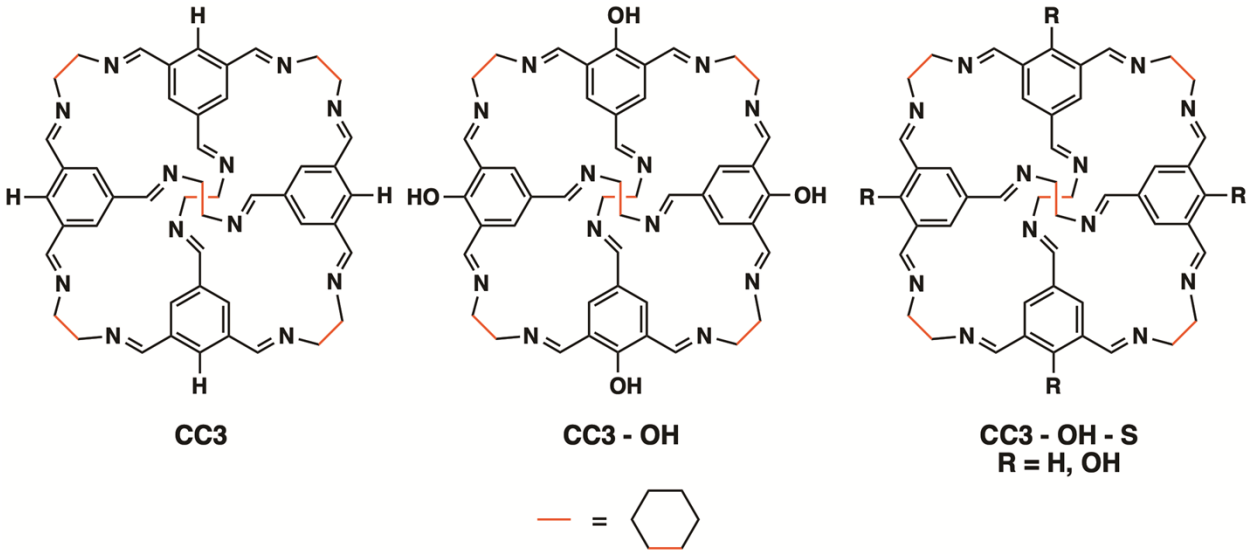

Figure 2. Molecular structures of the (left) CC3, (middle) CC3-OH, and (right) CC3-OH-S (scrambled CC3-OH) POCs that were evaluated.

Matrix-assisted laser desorption ionization (MALDI) mass spectrometry (MS) was employed (details in the SI) to further evaluate the presence of scrambled core functionalities. A cationizing agent was used to increase ion count as the cages were initially expected to produce positive ions. However, MALDI-MS results in negative ion mode identified several groups of five peaks in the expected mass-to-charge ratio (*m/z)* range that are associated with the presence of the cages. The first peak was observed at 1009.36 *m/z* and is followed by four peaks, each separated by 16 *m/z*, corresponding to the addition of a single –OH group. Positive and negative ion mode MALDI spectra of these POCs are shown in Figures S1 and S2. **To the best of our knowledge, this is the first report of scrambled core functionalities on POCs.**

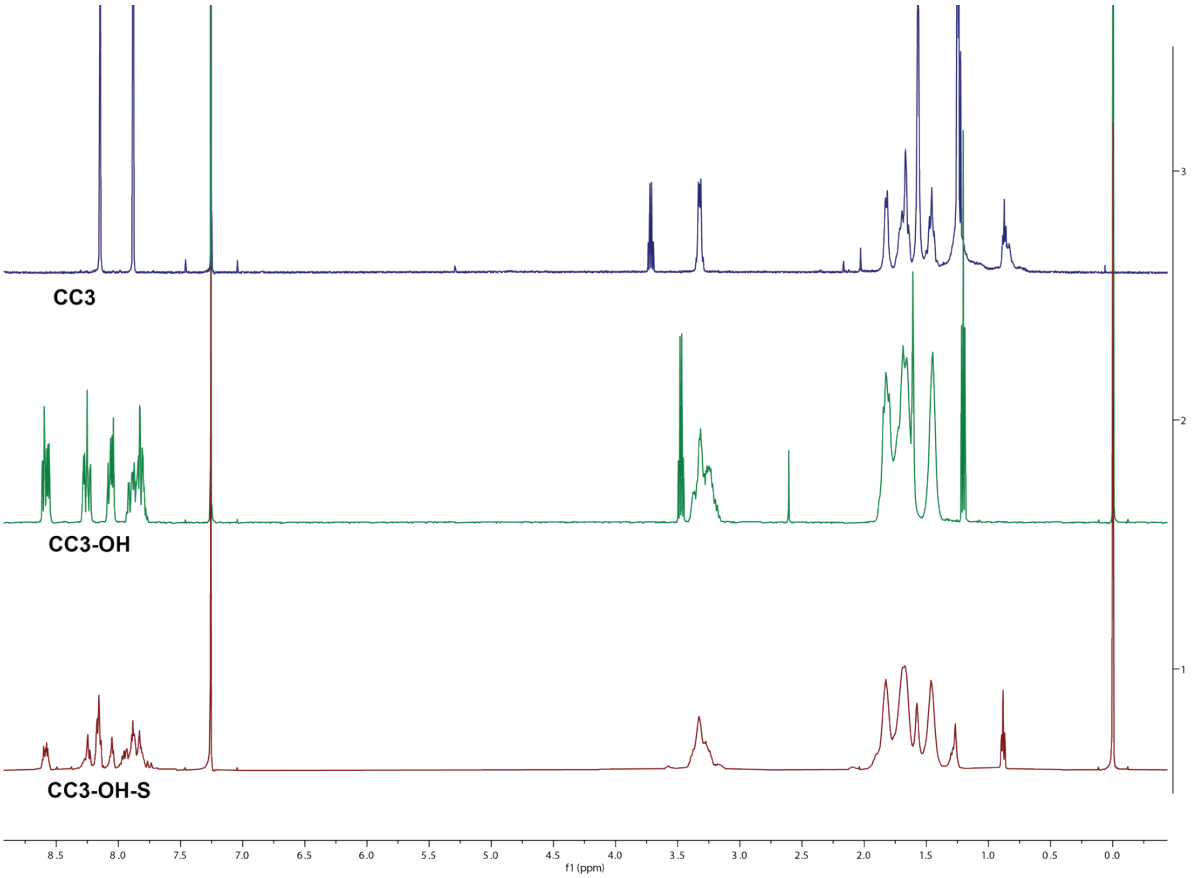

Figure 3. ^{1}H NMR comparison between CC3, CC3-OH, and CC3-OH-S POC structures, with peak broadening and multiplicity is indicative of scrambled structures.

Core scrambling of the CC3 POCs had a significant impact on the gas uptake properties. CO_2 absorption of the bulk POC solids were performed using standard methods at 0 °C and 25 °C (Figure 4). At both temperatures, the gas uptake of the POCs followed the trend of CC3-OH-S > CC3-OH > CC3. At 25°C the CC3-OH POC exhibited a 20% increase in CO_2 adsorption compared with the CC3 POC, while the CC3-OH-S was 40% higher than the CC3 POC. The effect of the scrambling was even stronger at lower temperatures (0°C), with the introduction of hydroxides creating a 9% increase in CO_2 adsorption compared with the CC3 POC, compared to a 62% increase for the CC3-OH-S POC. The increased CO_2 adsorption at lower temperatures suggests that changes in binding site strength and accessibility are a primary mechanism, since at elevated temperatures kinetic effects, such as gas diffusion may dominate, decreasing the effectiveness of these mechanisms.

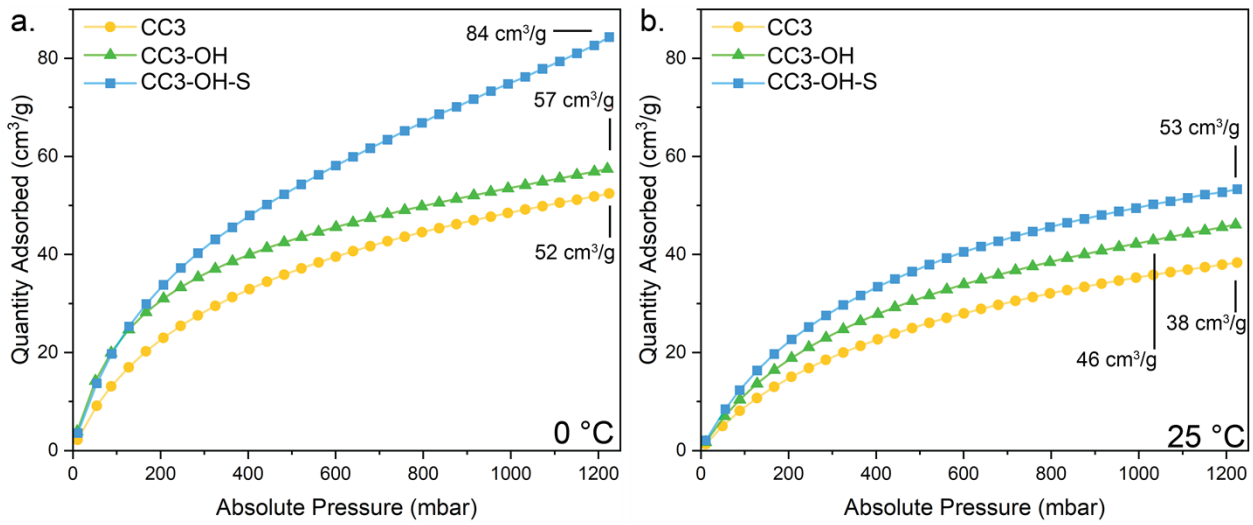

Figure 4: CO_2 adsorption (cm^3/g) for bulk solid CC3 (yellow circles), CC3-OH (green triangles), and CC3-OH-S (blue squares) structure at (a) 0˚C and (b) 25˚C.

Following analysis of the bulk solids, the POCs were combined with solvents to form PLs to identify how solvation of the POC structures impacted their gas adsorption performance. Each POC (CC3, CC3-OH, or CC3-OH-S) was formulated into an approximately 10 wt% PL system using Invoil 704 as a size excluded solvent. The silicon oil Invoil 704, consisting of 1,3,3,5-tetramethyl-1,1,5,5-tetraphenyltrisiloxane, was selected for its ultra-low vapor pressure and large molecular size[28] since PL formation requires a solvent sterically excluded from the interior of the porous material[27, 42]. The neat solvent as well as the PL formulation were analyzed for CO_2 uptake capacity (Figure 5). The neat Invoil 704 displayed minimal CO_2 capture at both 0°C and 25°C and matched well with previous reported uptakes[28]. In contrast, the PLs had dramatically higher gas adsorption, confirming the existence of gas accessible porosity, and thus PL formulation.

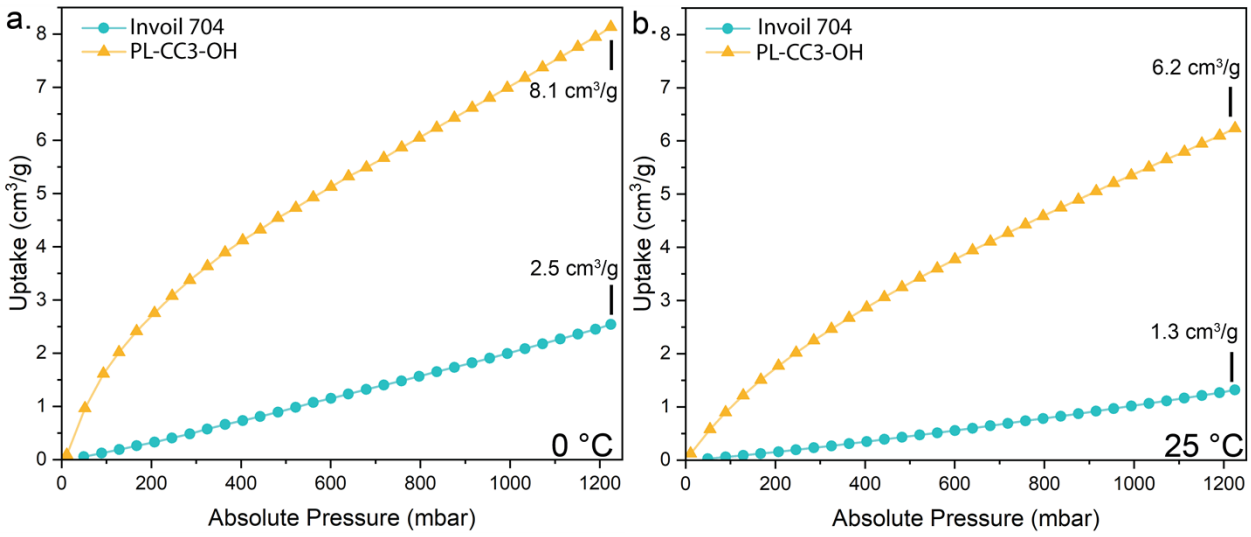

Figure 5: Exemplar CO_2 adsorption (cm^3/g) of neat solvent (Invoil 704, teal circles) and 10 wt% CC3-OH + Invoil 704 (yellow triangles) based PL at (a) 0˚C and (b) 25˚C.

To account for the incorporation of the sorbent, the CO_2 uptake of POC-based PLs was adjusted for the mass of the POC in solution (Figure 6), allowing for standardization of the PL by concentration of the POC. This analysis allowed us to determine if the POC uptake behavior differs in the PLs when compared to the bulk solid. The results identified that the CO_2 uptake of the CC3 and CC3-OH did not substantially change in the PL as compared to their bulk solids. However, CC3-OH-S showed a significant deviation from its bulk behavior. PLs formulated with CC3-OH-S exhibited an increase in the CO_2 uptake when compared to the bulk (Figure 7). At 0°C, CC3-OH-S based PLs exhibited a CO_2 uptake of 117 cm^3/g at 1.25 bar, at 25 °C the same formulations showed a CO_2 uptake of 85 cm^3/g at 1.25 bar, a twofold increase in the uptake capacity of CC3 based PLs at 0°C.

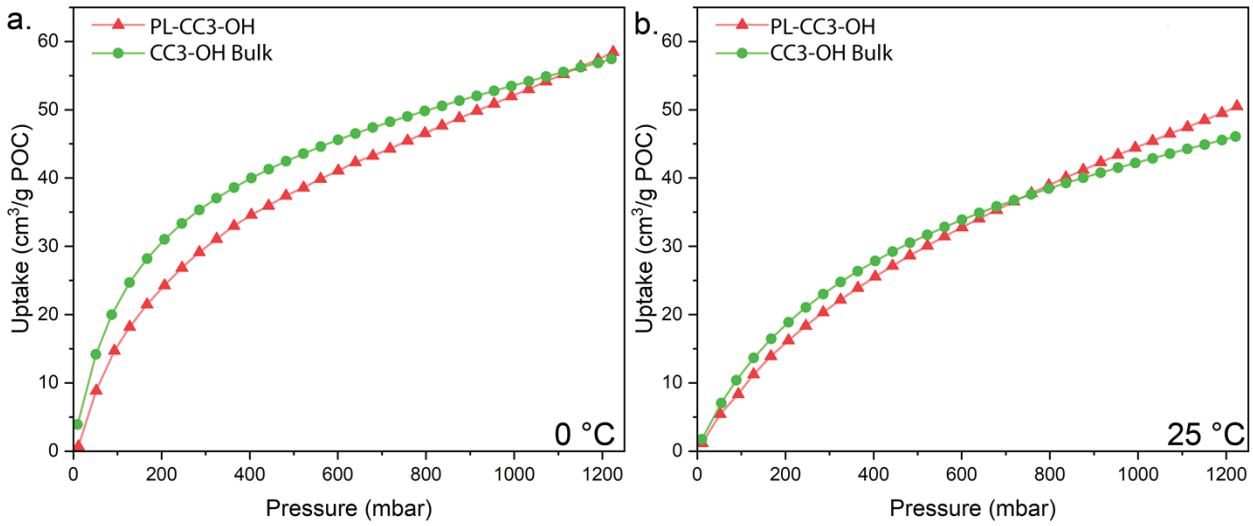

Figure 6: CO_2 uptake of bulk CC3-OH POC (green circles) and in the 10 wt% CC3-OH + Invoil 704 PL (red triangles) per-mass of the POC at (a) 0˚C and (b) 25˚C.

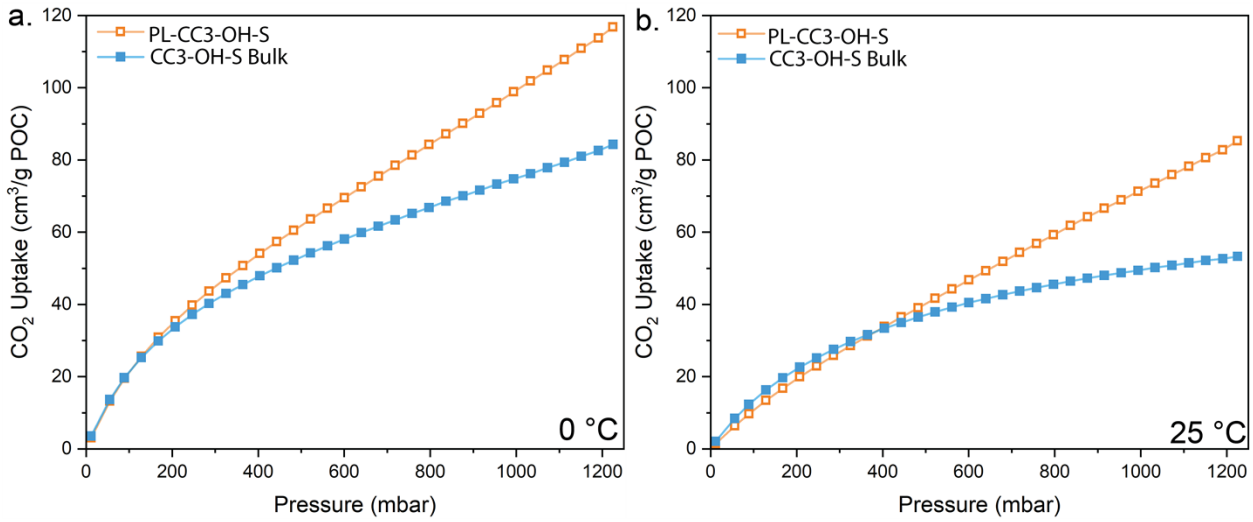

Figure 7: CO_2 uptake of bulk CC3-OH-S POC (solid blue squares) and in the 8.88 wt% CC3-OH-S + Invoil 704 PL (open orange squares) per-mass of the POC at (a) 0˚C and (b) 25˚C.

The increase in CO_2 adsorption in the CC3-OH-S scramble-based PL suggests that new or stronger binding sites are being developed, in comparison to the CC3 or CC3-OH structures. DFT simulations of CO_2 binding with the CC3 and CC3-OH derivatives were used to identify mechanisms of increased CO_2 uptake in the PLs.

Gas capture in porous materials can be controlled primarily through two mechanisms, the first is via diffusion through the pore window, through which molecular sieving occurs. The second

is via the pore volume, which controls the number of gas molecules that are thermodynamically stable in the pore and alters the gas adsorption capacity. Both features of the POCs were evaluated for their impact on CO_2 binding. Additionally, two configurations of the POCs were evaluated. In the first, the POCs exhibit intramolecular bonding between the hydroxide and the neighboring imine bond, termed "imine bound". In the second, the hydroxides in the POC are rotated 180° and oriented toward the hydrogen on the neighboring benzene ring, termed "free OH". Previous reports in crystalline functional materials have noted the strong influence on intramolecular hydrogen bonding[41] in controlling gas adsorption properties, necessitating that it is considered in this analyses.

First, we evaluated the thermodynamic binding energies of a single CO_2 molecule in the pore window of the CC3 POC with increase core hydroxide content. Generally, the focus of gas binding in PLs has been on binding sites inside the POC, since this has been assumed to be the driver for increased CO_2 adsorption capacity. Yet, previous DFT studies of gas binding in POCs have indicated that binding inside the pore window is the strongest site for both gas molecules and coordinating solvents in the CC13 POC[34]. Additionally, the core scrambling may alter the size and geometry of the pore window, relative to vertex scrambling. Therefore, we evaluated the impact of hydroxide core scrambling on CO_2 binding in CC3 POCs. Figure 8 provides snapshots of the pore windows in the CC3 and CC3-OH POC with varying levels of hydroxide content (33%, 66%, and 100%). Note that in all these snapshots the hydroxides are oriented toward the neighboring imine.

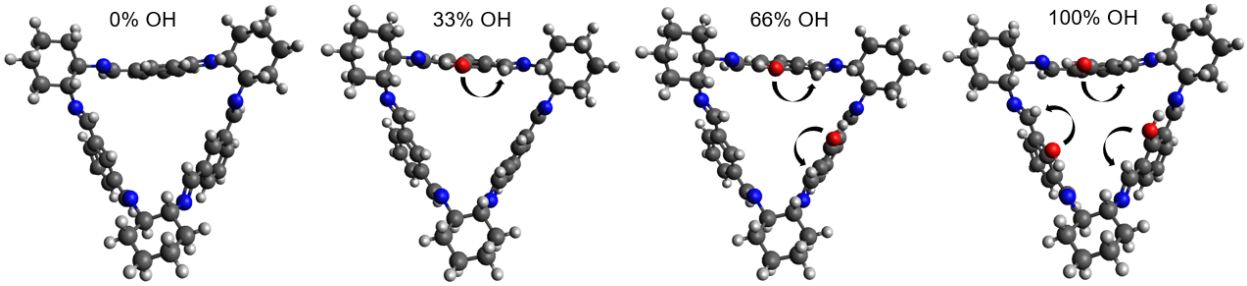

Figure 8: Snapshots of CC3-OH possible pore window configurations with 0%-100% OH substitution of the POC linker. The arrow indicates where hydrogen bond rotation could occur in these molecules. Atom colors: carbon (grey), oxygen (red), nitrogen (blue), and hydrogen (white).

Overall, a favorable binding energy of –20 to –22 kJ/mol was found for CO_2 binding in the pore window (Table 1). Interestingly, despite the increase core hydroxide content of the POC, there is minimal effect on CO_2 binding in the pore window. The slightly stronger CO_2 binding in the 66% hydroxide CC3-OH POCs, with a reduction of the CO_2 binding energy by 2 to 4 kJ/mol, is within the error of the calculation. The lack of effect of the core hydroxide content on the CO_2 binding in the pore window is driven by the preferred hydroxide binding with either the neighboring imine or the neighboring aryl hydrogen, so that the hydroxide is not available for stronger binding with the CO_2, effectively generating identical binding environments in the pore window. A snapshot of this binding geometry is included in Figure 9.

Table 1: Binding energy (kJ/mol) for a CO_2 molecule in pore window of the CC3 and CC3-OH POCs with either the hydroxide bound (imine-bound) or not bound (free-OH) to the neighboring imine.

Binding Site	**Imine-Bound (kJ/mol)**	**Free-OH (kJ/mol)**
0%	–25	–25
33%	–25	–24
66%	–28	–30
100%	–24	–26

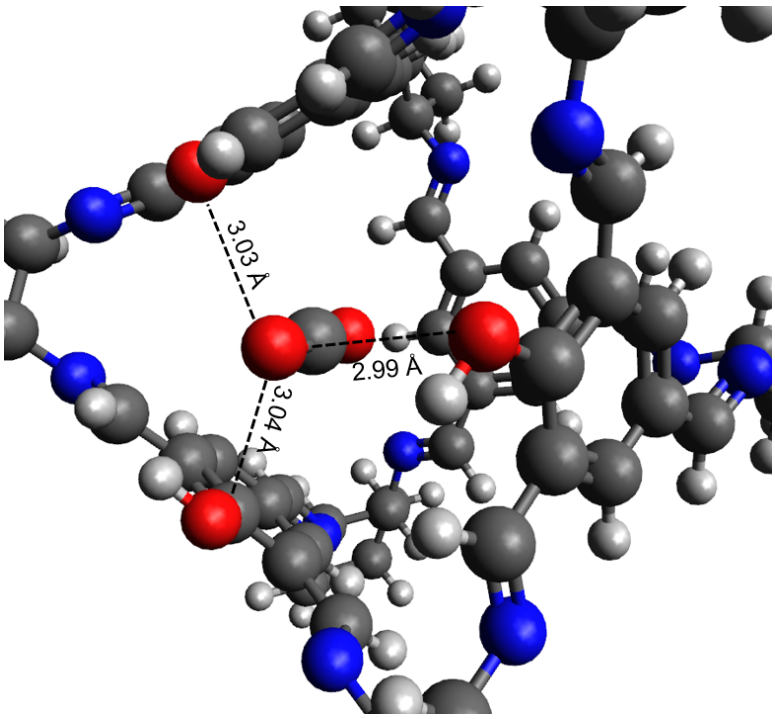

Figure 9: CO_2 binding in the pore window of CC3-OH with 100% OH content. All OH are oriented toward the hydrogen on the neighboring benzene ring. Interatomic distances between the oxygen in the CO_2 molecule and the oxygen in the hydroxide are included. Atom colors: carbon (grey), oxygen (red), nitrogen (blue), and hydrogen (white).

Second, we evaluated the thermodynamic binding energy of CO_2 in the POC pore. The per-molecule binding energies for CO_2 in the interior pore of the CC3 POC with 0%, 33%, 66%, and 100% hydroxide content is included in Table S1. Overall, the per-molecule binding energies for structures was negative, indicating a thermodynamic drive for gas binding. Additionally, per-molecule binding energies varied between –23 and –34 kJ/mol, all indicative of physisorption binding mechanisms[38]. For both the imine-bound and free-OH POC intramolecular structures, the binding energies increase with increasing hydroxide concentration. This behavior is significantly stronger in the case when the hydroxide is not intramolecularly bound to the cage (free hydroxide). For zero hydroxide content (CC3), the average CO_2 binding energy in the pore is -24 kJ/mol and then increases to –33 kJ/mol for fully hydroxide POC (CC3-OH 100%), as seen in Figure 10.

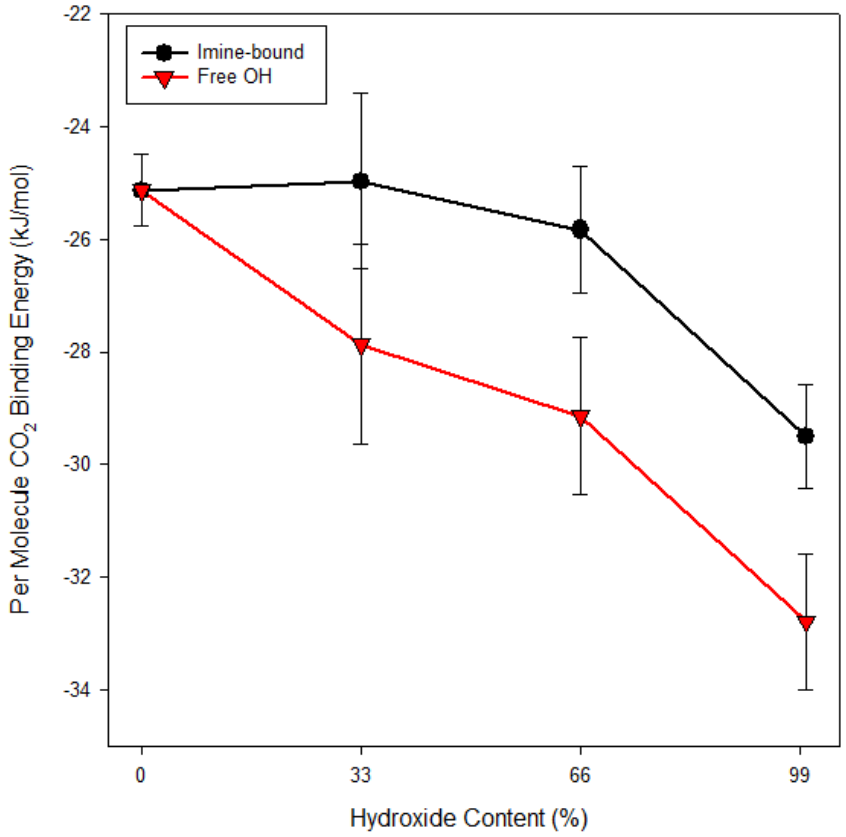

Figure 10: Per molecule CO_2 binding energy (kJ/mol) for CO_2 in the POC pore versus increasing hydroxide content of the CC3 POCs. Results are averaged between structure with hydroxides that are intramolecular bound to the neighboring imine and those that contain free hydroxides and from one to seven CO_2 molecules in the pore. The standard deviation of the data is also reported, and the individual data is included in Table S1.

The stronger binding in the POC when the hydroxides are not interacting with the neighboring amine is driven by the nanoconfinement of the CO2 molecules in the cage. Evaluation of CO_2 binding structures in the POCs found that as the number of CO_2 molecules in the pore increases, the gas molecules are pushed out of their preferred binding configuration in the center of the pore. Instead, the CO_2 interact directly with the linker hydroxide in the window (see a snapshot in Figure 11), leading to the increase in average CO_2 binding energy. In contrast when the hydroxide is interacting with the neighboring imines the CO_2 molecules are forced out of the POC and bind with the exterior. The difference in CO_2 binding behavior is driven by the strong

interaction between the hydroxide and the neighboring imine, which does not rotate to interact with the CO_2 molecule as it exits the pore.

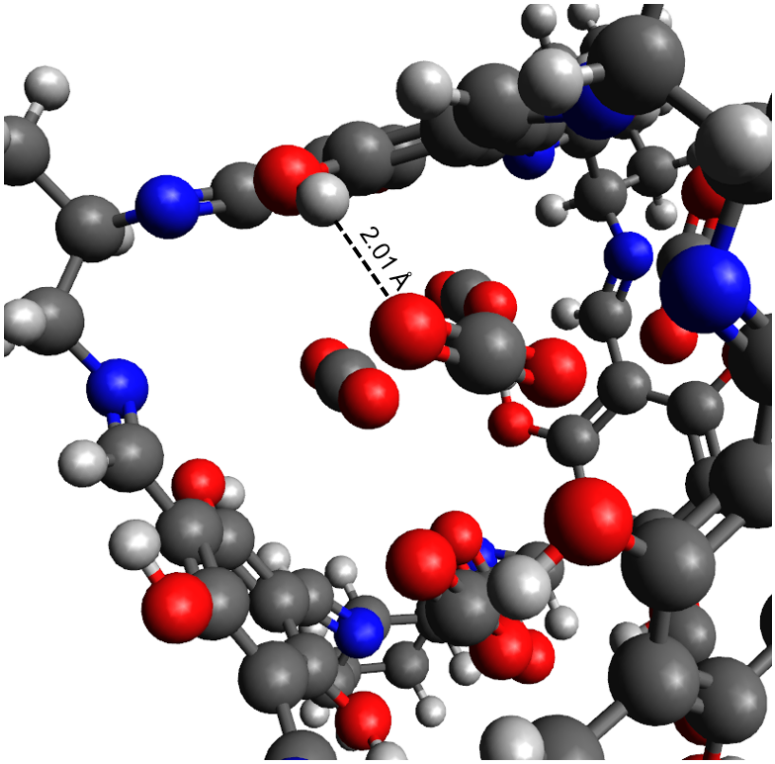

Figure 11: CO_2 binding with the hydroxide in the CC3-OH POC (100% OH content). Distance between the oxygen in the CO_2 and the hydrogen in the hydroxide is included. Atom colors: carbon (grey), oxygen (red), nitrogen (blue), and hydrogen (white).

To further explore this mechanism, single point calculations of the POC following CO_2 adsorption was performed and compared with the empty POC to isolate effects on the cage structure following infiltration. As the POC is filled with CO_2 molecules, the trapped gases cause pressure on the POC, causing an increase in energy relative to the fully relaxed and empty POC. As seen in Figure 12, this strain energy from filling the CC3-OH POCs with CO_2 molecules is higher for the POCs in the free-OH configuration compared to the imine-bound configuration, due to the forced interactions with the hydroxides as the interior pore fills for the free-OH configuration. These results showed that configuration of core hydroxides within CC3-OH POCs governs the strength of CO_2 binding with the POC. Scrambling of the CC3-OH POC during

synthesis may release the hydroxide from intramolecular binding with the neighboring imine, allowing for stronger direct hydroxid-CO_2 interactions.

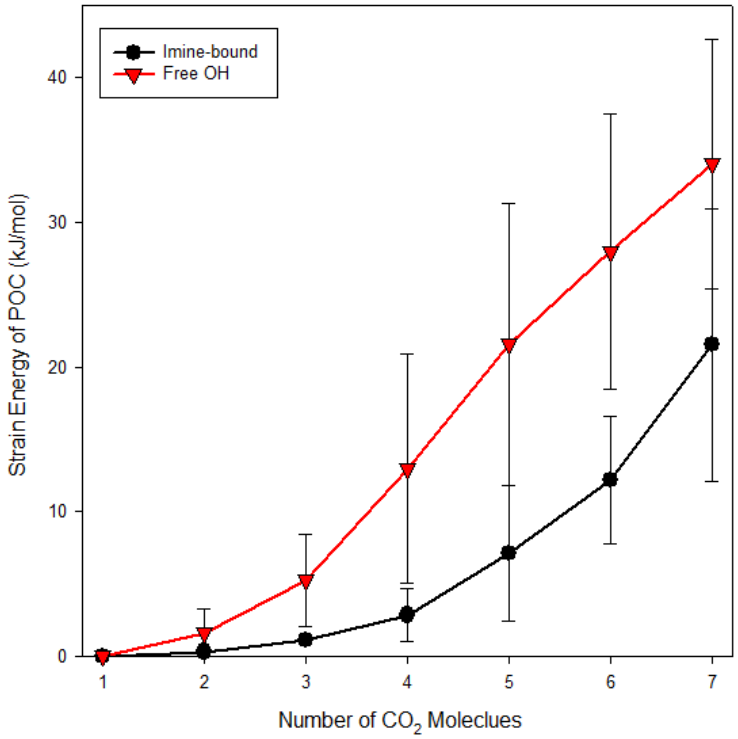

Figure 12: Strain energy (kJ/mol) of the POC with increasing number of CO_2 molecules in the primary pore. Results are separated by POCs that contain imine-bound or free hydroxides and averaged over the amount of hydroxide per linker. Individual data is in the SI as Table S2.

IV. Discussion

Comparison of these results to previously reported Type II PLs indicate that scrambling the core linker results in an outsized impact on the functional properties of the PL. Comparison with CO_2 uptake in PLs formed from similar POCs by Kai et al.[43], including the vertex functionalized CC3 POCs, found CO_2 uptakes at 25°C and 1 bar of ~4.5 cm^3/g, below the 7 cm^3/g for the PL-CC3-OH-S composition identified here. Similarly, variation of the porous host materials, for example through use of the zeolitic imidazolate frameworks (ZIF) class of metal–organic frameworks with the same solvent (Invoil 704) identified that other common porous host materials (ZIF-8, ZIF-7, and Mg-IRMOF-74) did not exhibit the same performance as the CC3-OH-S[28] as

seen in Figure 13. This observation highlights the delicate balance between the properties of the nanoporous materials and the surrounding solvent in enabling high-capacity gas adsorption.

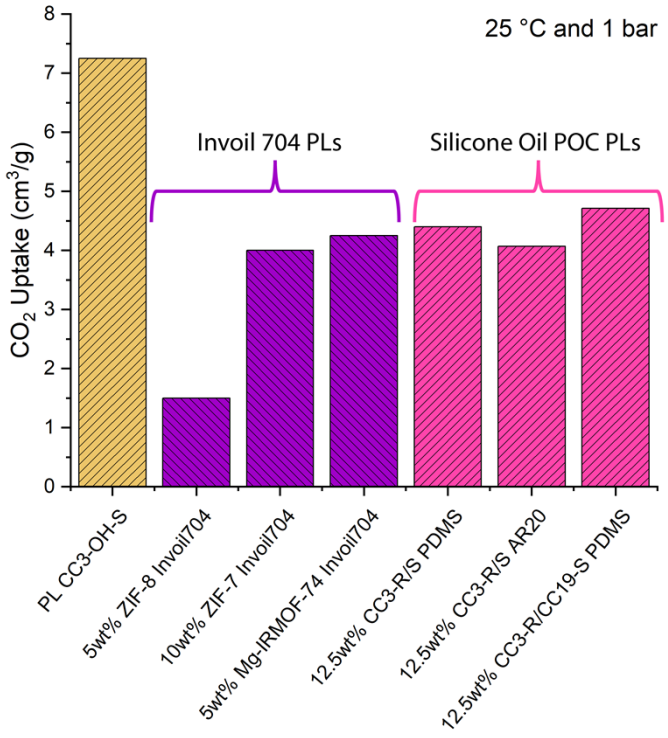

Figure 13: Comparison of CO_2 uptake (cm^3/g) for the 10 wt% PL-CC3-OH-S compared with previous studies with the same solvent (Invoil 704) or the CC3 family of POCs[43].

A key question in the industrial application of the PLs is their cyclability and the potential regeneration cost. Cyclic CO_2 adsorption experiments were performed to evaluate how repeated gas adsorption cycles performed. Results in Figure 14 indicate that repeated CO_2 adsorption cycling resulted in decreasing adsorption. CC3 based PLs lost between 1-2% of CO_2 capacity per adsorption cycle (Figure 14), indicating that more rigorous regeneration conditions may be necessary to fully reactivate the samples. While pristine CC3 based PL showed the best cyclability of the series, the CC3-OH-S system showed the lowest cyclability. The larger decrease in adsorption performance is attributed to a higher binding affinity for CO_2, indicating that stronger thermodynamic binding sites limit the ability of the CO_2 to desorb.

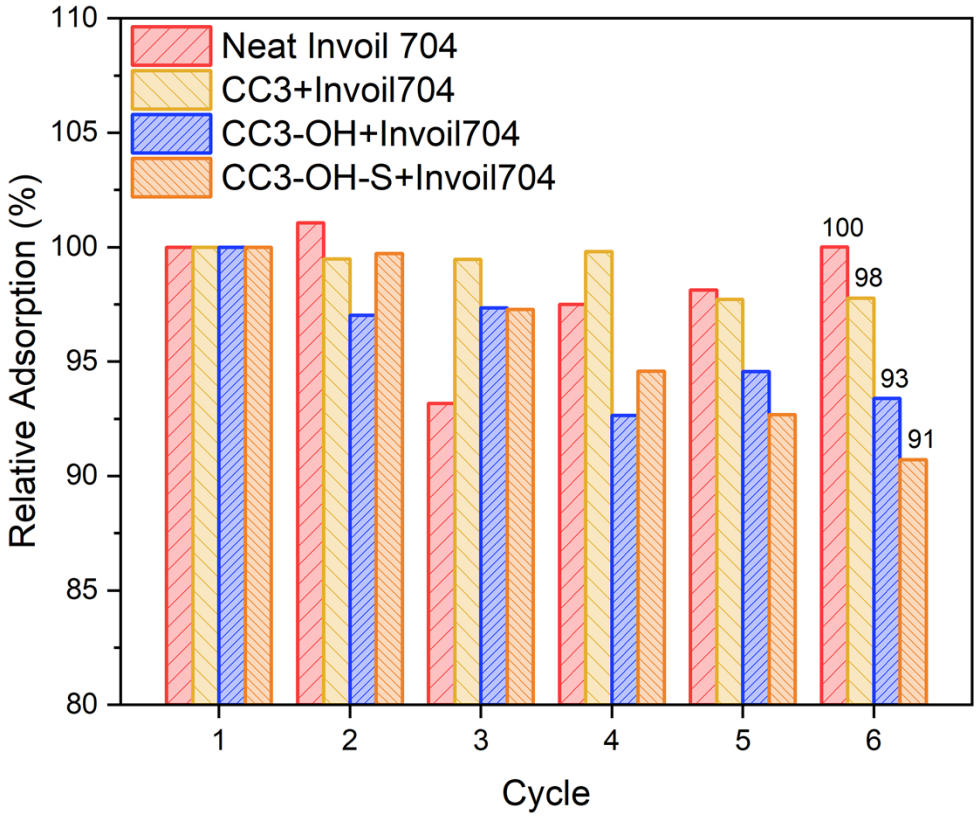

Figure 14: Cyclability of CC3-based PLs as a function of relative adsorption.

V. CONCLUSION

Herein, we have demonstrated how the position and degree of substitution of POC synthetic modifications impacts the functional properties of POCs and resulting PLs. While the impact of -OH substitution on the core of CC3 based POCs has been evaluated, we found that scrambled POC structures display a significant increase in the CO_2 adsorption capacity, both as bulk powders and as PLs. While -OH functionalization at every core in the POC (CC3-OH) results in an increase in the overall CO_2 uptake of the system, scrambling the core to include -OH and -H functionalities result in an emergent property in PL systems. We believe this is due to the accessibility of the pore as well as providing a robust binding site for adsorbed gasses. While periphery scrambled systems have previously been described, this is the first time to our knowledge that core scrambled POCs have been characterized and evaluated as gas sorbents. Density functional theory calculations of the CC3 POC and hydroxide derivatives identified that the orientation of the hydroxides on the

linker, either oriented towards or away from the neighboring imine, significantly altered the CO_2 binding energy. CC3 POCs with OH oriented away from the imine exhibited stronger CO_2 binding with higher hydroxide content, while the POCs with the hydroxide oriented toward the imine did not exhibit changes in CO_2 binding. Therefore, solvation of the CC3 and CC3-OH POC introduced stronger binding by reorienting the hydroxides on the linker. These results uncover a key structural relationship of CC3-OH POCs that enables emergent gas capture properties in PLs to guide future development and discovery of PLs for targeted gas capture and separation applications.

Supporting Information.

Supporting information includes the negative ion mode MALDI spectra for three samples of the CC3-OH-S POC structures (Figure S1) and the corresponding positive ion mode data (Figure S2), the ^{1}H NMR of the CC3-OH-S POC (Figure S3), per molecule CO_2 binding energy with the CC3 POC (0%) and with CC3-OH POCs with increasing hydroxide content (Table S1), strain energy for single point calculations of the CC3 POC (0%) and with CC3-OH POCs with increasing hydroxide content (33%, 66%, and 100%) filled with 1-7 CO_2 molecules (Table S2), and the atomic coordinates of the CC3 POC and the hydroxide derivatives.

Corresponding Author

*Jessica Rimsza – jrimsza@sandia.gov

Present Addresses

†Matthew J. Hurlock, matthew.hurlock@pnnl.gov, Pacific Northwest National Laboratory, Richland, Washington

Author Contributions

The manuscript was written through contributions of all authors. All authors have given approval to the final version of the manuscript. HDR – conceptualization, formal analysis, investigation, resources, data curation, writing - original draft, writing – reviewing & editing, funding acquisition. MJH – formal analysis, investigation, data curation, writing - original draft, writing – reviewing & editing. NRB – formal analysis, data curation, writing – reviewing & editing. BMA –data curation, writing – reviewing & editing. JMR – conceptualization, formal analysis, investigation, resources, data curation, writing - original draft, writing – reviewing & editing, project administration, funding acquisition.

Funding Sources

This work was supported by Sandia National Laboratory (SNL) Laboratory Directed Research and Development (LDRD) project #230709.

ACKNOWLEDGMENT

We thank Matthew S. Christian of Sandia National Laboratories for a detailed technical review and thoughtful comments. This article has been authored by an employee of National Technology & Engineering Solutions of Sandia, LLC, under Contract No. DE-NA0003525 with the U.S. Department of Energy (DOE). The employee owns all right, title, and interest in and to the article and is solely responsible for its contents. The United States Government retains and the publisher, by accepting the article for publication, acknowledges that the United States Government retains a non-exclusive, paid-up, irrevocable, world-wide license to publish or reproduce the published form of this article or allow others to do so, for United States Government purposes. The DOE will provide public access to these results of federally sponsored research in accordance with the DOE Public Access Plan https://www.energy.gov/downloads/doe-public-access-plan.

REFERENCES:

(1) Sholl, D. S.; Lively, R. P. Seven chemical separations to change the world. *Nature* **2016**, *532* (7600), 435-437.

(2) Sholl, D. S.; Lively, R. P. Exemplar mixtures for studying complex mixture effects in practical chemical separations. *J. Amer. Chem. Soc. Au* **2022**, *2* (2), 322-327.

(3) Jia, T.; Gu, Y.; Li, F. Progress and potential of metal-organic frameworks (MOFs) for gas storage and separation: A review. *J. Environ. Chem. Eng.* **2022**, *10* (5), 108300.

(4) Tao, Y.; Xu, H. A critical review on potential applications of Metal-Organic frameworks (MOFs) in adsorptive carbon capture technologies. *Appl. Therm. Eng.* **2024**, *236*, 121504.

(5) Zeng, Y.; Zou, R.; Zhao, Y. Covalent organic frameworks for CO_2 capture. *Adv. Mater.* **2016**, *28* (15), 2855-2873.

(6) Li, H.; Dilipkumar, A.; Abubakar, S.; Zhao, D. Covalent organic frameworks for CO_2 capture: from laboratory curiosity to industry implementation. *Chem. Soc. Rev.* **2023**, *52* (18), 6294-6329.

(7) Tozawa, T.; Jones, J. T.; Swamy, S. I.; Jiang, S.; Adams, D. J.; Shakespeare, S.; Clowes, R.; Bradshaw, D.; Hasell, T.; Chong, S. Y. Porous organic cages. *Nat. Mater.* **2009**, *8* (12), 973-978.

(8) Hasell, T.; Cooper, A. I. Porous organic cages: soluble, modular and molecular pores. *Nat. Rev. Mater.* **2016**, *1* (9), 1-14.

(9) Hasell, T.; Chong, S. Y.; Jelfs, K. E.; Adams, D. J.; Cooper, A. I. Porous organic cage nanocrystals by solution mixing. *J. Amer. Chem. Soc.* **2012**, *134* (1), 588-598.

(10) Mintova, S.; Jaber, M.; Valtchev, V. Nanosized microporous crystals: emerging applications. *Chem. Soc. Rev.* **2015**, *44* (20), 7207-7233.

(11) Dai, C.; Qian, H.-L.; Yan, X.-P. Facile room temperature synthesis of ultra-small sized porous organic cages for fluorescent sensing of copper ion in aqueous solution. *J. Hazard. Mater.* **2021**, *416*, 125860.

(12) La Cognata, S.; Amendola, V. Recent applications of organic cages in sensing and separation processes in solution. *Chem. Commun.* **2023**, *59* (92), 13668-13678.

(13) Yang, X.; Sun, J.-K.; Kitta, M.; Pang, H.; Xu, Q. Encapsulating highly catalytically active metal nanoclusters inside porous organic cages. *Nat. Catal.* **2018**, *1* (3), 214-220.

(14) Borse, R. A.; Tan, Y.-X.; Yuan, D.; Wang, Y. Progress of porous organic cages in photo/electrocatalytic energy conversion and storage applications. *Energy Environ. Sci.* **2024**, *17* (4), 1307-1329.

(15) Wang, W.; Su, K.; Yuan, D. Porous organic cages for gas separations. *Mater. Chem. Front.* **2023**, *7* (21), 5247-5262.

(16) Kewley, A.; Stephenson, A.; Chen, L.; Briggs, M. E.; Hasell, T.; Cooper, A. I. Porous organic cages for gas chromatography separations. *Chem. Mater.* **2015**, *27* (9), 3207-3210.

(17) Giri, N.; Del Pópolo, M. G.; Melaugh, G.; Greenaway, R. L.; Rätzke, K.; Koschine, T.; Pison, L.; Gomes, M. F. C.; Cooper, A. I.; James, S. L. Liquids with permanent porosity. *Nature* **2015**, *527* (7577), 216-220.

(18) Jiang, S.; Jones, J. T.; Hasell, T.; Blythe, C. E.; Adams, D. J.; Trewin, A.; Cooper, A. I. Porous organic molecular solids by dynamic covalent scrambling. *Nat. Commun.* **2011**, *2* (1), 207.

(19) Evans, J. D.; Sumby, C. J.; Doonan, C. J. Synthesis and applications of porous organic cages. *Chem. Lett.* **2015**, *44* (5), 582-588.

(20) Berardo, E.; Greenaway, R. L.; Turcani, L.; Alston, B. M.; Bennison, M. J.; Miklitz, M.; Clowes, R.; Briggs, M. E.; Cooper, A. I.; Jelfs, K. E. Computationally-inspired discovery of an unsymmetrical porous organic cage. *Nanoscale* **2018**, *10* (47), 22381-22388.
(21) Greenaway, R. L.; Jelfs, K. E. High-Throughput Approaches for the Discovery of Supramolecular Organic Cages. *ChemPlusChem* **2020**, *85* (8), 1813-1823.
(22) Jiang, S.; Du, Y.; Marcello, M.; Corcoran, E. W., Jr.; Calabro, D. C.; Chong, S. Y.; Chen, L.; Clowes, R.; Hasell, T.; Cooper, A. I. Core-Shell Crystals of Porous Organic Cages. *Angew Chem Int Ed Engl* **2018**, *57* (35), 11228-11232.
(23) Petryk, M.; Szymkowiak, J.; Gierczyk, B.; Spolnik, G.; Popenda, L.; Janiak, A.; Kwit, M. Chiral, triformylphenol-derived salen-type [4 + 6] organic cages. *Org Biomol Chem* **2016**, *14* (31), 7495-7499.
(24) Yuan, Y. D.; Dong, J.; Liu, J.; Zhao, D.; Wu, H.; Zhou, W.; Gan, H. X.; Tong, Y. W.; Jiang, J.; Zhao, D. Porous organic cages as synthetic water channels. *Nat Commun* **2020**, *11* (1), 4927.
(25) Hurlock, M. J.; Christian, M. S.; Fritzsching, K. J.; Rademacher, D. X.; Rimsza, J. M.; Nenoff, T. M. Experimental and computational mechanisms that govern long-term stability of CO_2-adsorbed ZIF-8-based porous liquids. *ACS Appl. Mater. Inter.* **2023**, *15* (27), 32792-32802.
(26) Hurlock, M. J.; Christian, M. S.; Rimsza, J. M.; Nenoff, T. M. Design Principles Guiding Solvent Size Selection in ZIF-Based Type 3 Porous Liquids for Permanent Porosity. *ACS Materials Au* **2023**, *4* (2), 224-237.
(27) Hurlock, M. J.; Lu, L.; Sarswat, A.; Chang, C.-W.; Rimsza, J. M.; Sholl, D. S.; Lively, R. P.; Nenoff, T. M. Exploitation of Pore Structure for Increased CO_2 Selectivity in Type 3 Porous Liquids. *ACS Appl. Mater. Interfaces* **2024**, *16* (38), 51639-51648.
(28) Koutsianos, A.; Pallach, R.; Frentzel-Beyme, L.; Das, C.; Paulus, M.; Sternemann, C.; Henke, S. Breathing porous liquids based on responsive metal-organic framework particles. *Nat. Commun.* **2023**, *14* (1), 4200.
(29) Hurlock, M. J.; Lu, L.; Huang, C.; Rimer, J.; Lively, R. P.; Rimsza, J.; Nenoff, T. M. Structure-Property Relationships of Nanozeolite-Based Porous Liquids for Carbon Capture. *J. Mol. Liq.* **2025**.
(30) Kresse, G.; Hafner, J. Ab initio molecular dynamics for liquid metals. *Phys. Rev. B* **1993**, *47* (1), 558-561.
(31) Kresse, G.; Hafner, J. Ab initio molecular-dynamics simulation of the liquid-metal--amorphous-semiconductor transition in germanium. *Phys. Rev. B* **1994**, *49* (20), 14251-14269.
(32) Perdew, J. P.; Ruzsinszky, A.; Csonka, G. I.; Vydrov, O. A.; Scuseria, G. E.; Constantin, L. A.; Zhou, X.; Burke, K. Restoring the Density-Gradient Expansion for Exchange in Solids and Surfaces. *Phys. Rev. Lett.* **2008**, *100* (13), 136406.
(33) Grimme, S.; Antony, J.; Ehrlich, S.; Krieg, H. A consistent and accurate ab initio parametrization of density functional dispersion correction (DFT-D) for the 94 elements H-Pu. *J. Chem. Phys.* **2010**, *132* (15), 154104.
(34) Rimsza, J.; Nenoff, T. M. Design of enhanced porous organic cage solubility in Type 2 porous liquids. *J. Mol. Liq.* **2023**, *377*, 121536.
(35) Rimsza, J. M.; Chapman, K. W.; Nenoff, T. M. Influence of Al location on formation of silver clusters in mordenite. *Micropor. Mesopor. Mat.* **2021**, *327*, 111401.
(36) Rimsza, J. M.; Chapman, K. W.; Nenoff, T. M. Energetics and structure of Ag–water clusters formed in mordenite. *J. Phys. Chem. C* **2020**, *124* (8), 4517-4524.

(37) Sava Gallis, D. F.; Vogel, D. J.; Vincent, G. A.; Rimsza, J. M.; Nenoff, T. M. NOx adsorption and optical detection in rare earth metal–organic frameworks. *ACS Appl. Mater. Interfaces* **2019**, *11* (46), 43270-43277.
(38) Vogel, D. J.; Lee, Z. R.; Hanson, C. A.; Henkelis, S. E.; Smith, C. M.; Nenoff, T. M.; Dixon, D. A.; Rimsza, J. M. Predictive acid gas adsorption in rare earth DOBDC metal–organic frameworks via complementary cluster and periodic structure models. *J. Phys. Chem. C* **2020**, *124* (49), 26801-26813.
(39) Vogel, D. J.; Rimsza, J. M.; Nenoff, T. M. Prediction of Reactive Nitrous Acid Formation in Rare-Earth MOFs via ab initio Molecular Dynamics. *Angew. Chem.* **2021**, *133* (20), 11615-11623.
(40) Rimsza, J. M.; Nenoff, T. M. Critical role of solvation on CC13 porous organic cages for design of porous liquids. *J. Mol. Liq.* **2024**, *401*, 124731.
(41) Vogel, D. J.; Nenoff, T. M.; Rimsza, J. M. Tuned hydrogen bonding in rare-earth metal–organic frameworks for design of optical and electronic properties: an exemplar study of Y–2, 5-dihydroxyterephthalic acid. *ACS App. Mater. Interfaces* **2020**, *12* (4), 4531-4539.
(42) Robinson Brown, D.; Hurlock, M. J.; Nenoff, T. M.; Rimsza, J. M. Control of Permanent Porosity in Type 3 Porous Liquids via Solvent Clustering. *ACS Appl. Mater. Interfaces* **2025**.
(43) Kai, A.; Egleston, B. D.; Tarzia, A.; Clowes, R.; Briggs, M. E.; Jelfs, K. E.; Cooper, A. I.; Greenaway, R. L. Modular type III porous liquids based on porous organic cage microparticles. *Adv. Funct. Mater.* **2021**, *31* (51), 2106116.